JGR Space Physics

RESEARCH ARTICLE
10.1029/2023JA031882

Dependence of Electron Flux Dropouts in the Earth's Outer Radiation Belt on Energy and Driving Parameters During Geomagnetic Storms

Man Hua[1], Jacob Bortnik[1], and Donglai Ma[1]

[1]Department of Atmospheric and Oceanic Sciences, UCLA, Los Angeles, CA, USA

Key Points:

- We analyze the statistical dependence of the outer radiation belt electron flux dropouts on energy and various driving parameters
- Dropouts are naturally divided into three regions, showing higher occurrence at <100 keV and >1 MeV compared to the intermediate energies
- Dropouts at different energies and L-shells show various dependencies on magnetic local time, interplanetary magnetic field B_z, P_{SW}, SYM-H, and AE

Supporting Information:

Supporting Information may be found in the online version of this article.

Correspondence to:

M. Hua,
manhua@ucla.edu

Citation:

Hua, M., Bortnik, J., & Ma, D. (2023). Dependence of electron flux dropouts in the Earth's outer radiation belt on energy and driving parameters during geomagnetic storms. *Journal of Geophysical Research: Space Physics*, *128*, e2023JA031882. https://doi.org/10.1029/2023JA031882

Received 12 JUL 2023
Accepted 1 OCT 2023

Abstract Using 5-year of measurements from Van Allen Probes, we present a survey of the statistical dependence of the Earth's outer radiation belt electron flux dropouts during geomagnetic storms on electron energy and various driving parameters including interplanetary magnetic field B_z, P_{SW}, SYM-H, and AE. By systematically investigating the dropouts over energies of 1 keV–10 MeV at L-shells spanning 4.0–6.5, we find that the dropouts are naturally divided into three regions. The dropouts show much higher occurrence rates at energies below ∼100 keV and above ∼1 MeV compared to much smaller occurrence rate at intermediate energies around hundreds of keV. The flux decays more dramatically at energies above ∼1 MeV compared to the energies below ∼100 keV. The flux dropouts of electrons below ∼100 keV strongly depend on magnetic local time (MLT), which demonstrate high occurrence rates on the nightside (18–06 MLT), with the highest occurrence rate associated with northward B_z, strong P_{SW} and SYM-H, and weak AE conditions. The strongest flux decay of these dropouts is found on the nightside, which strongly depends on P_{SW} and SYM-H. However, there is no clear MLT dependence of the occurrence rate of relativistic electron flux dropouts above ∼1 MeV, but the flux decay of these dropouts is more significant on the dayside, with stronger decay associated with southward IMF B_z, strong P_{SW}, SYM-H, and AE conditions. Our statistical results are crucial for understanding of the fundamental physical mechanisms that control the outer belt electron dynamics and developing future potential radiation belt forecasting capability.

1. Introduction

A great number of groundbreaking discoveries of the Earth's radiation belt electron dynamics have been achieved since its discovery in 1958 (Li & Hudson, 2019; Ripoll et al., 2020; Tu et al., 2019), which is of great scientific and practical interest. These outer belt electrons range from tens of keV to several MeV, and can exhibit highly dynamic behavior, including loss, transport, and acceleration processes. Their flux change can reach several orders of magnitude with timescales varying from hours to days, especially during strong storm or substorm activity (Baker et al., 2004, 2019; Hua, Bortnik, Spence, & Reeves, 2023; Reeves et al., 2016; Turner et al., 2015, 2019). Among these processes, fast and strong decreases in electron fluxes, also called dropouts (Green et al., 2004; Onsager et al., 2002; Turner, Morley, et al., 2012, and references therein), have attracted extensive attention due to their essential importance for radiation belt modeling and prediction.

It has been well acknowledged that dropouts typically occur during storm events (e.g., Baker et al., 1994; Reeves et al., 2003; Xiang et al., 2018), and can be caused by various mechanisms operating individually or jointly. Magnetopause shadowing due to solar wind compression of the magnetopause (Bortnik et al., 2006; Kim & Chan, 1997; Ma et al., 2020; Staples et al., 2022; Turner, Shprits, et al., 2012; Ukhorskiy et al., 2006) or/and accompanied by enhanced outward radial diffusion (Ozeke et al., 2017, 2020; Shprits et al., 2006; Tu et al., 2019) can cause significant electron loss out of the magnetopause and into interplanetary space. Consequently, previous statistical studies (Boynton et al., 2016; Gao et al., 2015; Yuan & Zong, 2013) demonstrated that significant compression of the magnetosphere due to high solar wind dynamic pressure that leads to steep electron flux gradients and efficient outward radial diffusion creates a favorable condition to cause electron dropouts. Another important loss mechanism is precipitation into the upper atmosphere caused by pitch-angle scattering via interacting with various plasma waves, including whistler-mode chorus waves, electromagnetic ion cyclotron (EMIC) waves, and plasmaspheric hiss (Blum & Breneman, 2020; Clilverd et al., 2015; Lyu et al., 2022; Meredith et al., 2007; Miyoshi et al., 2008; Roger et al., 2015; Thorne, 2010; Thorne et al., 2010; Usanova et al., 2014). In addition, electron pitch-angle scattering can also occur when the magnetic field line around which electron

gyrates is highly stretched so that the electron gyroradius is comparable to the radius of field line curvature (Sergeev & Tsyganenko, 1982). This mechanism, also known as current sheet scattering (CCS), typically occurs on the nightside near the electron trapping boundary (outer radiation belt boundary), which can cause isotropic pitch-angle distribution and precipitation of relativistic electrons (Capannolo et al., 2022; Delcourt et al., 1996; Gray & Lee, 1982; Imhof et al., 1991, 1993; Smith et al., 2016; Yahnin et al., 2016, 2017). CCS primarily acts on electrons at higher energies compared to the lower energies due to the larger gyroradii of the high-energy electrons. Apart from these "true" loss processes, an adiabatic loss process, also known as the Dst effect, can also cause apparent electron dropouts during geomagnetic storms (Kim & Chan, 1997). During the adiabatic process, electrons move outward in L-shell and decrease in energy to conserve the three adiabatic invariants during the storm time due to the decrease of the geomagnetic field strength outside of the main ring current region when the ring current is enhanced. At least in principle, when the ring current decays, this process would reverse and these energetic electrons should move back to their original locations and energies.

Despite a great number of both observational and modeling studies having successfully explained the physical processes during electron flux dropouts in different events (e.g., Bortnik et al., 2006; Drozdov et al., 2019, 2022; George et al., 2022; Kang et al., 2018; Su et al., 2016; Tsurutani et al., 2016; Tu et al., 2014, 2019; Turner, Shprits, et al., 2012; Turner et al., 2014; Xiang et al., 2017; Zhang, Li, Ma, et al., 2016; Zhang, Li, Thorne, et al., 2016), only a limited number of studies systematically investigated the statistical distributions of the outer belt electron flux dropouts and their dependence on energies, various geomagnetic indices, and solar wind parameters. Several studies have demonstrated the important impact of the high solar wind dynamic pressure (P_{SW}) and southward interplanetary magnetic field (IMF) B_z on producing significant electron flux dropouts (e.g., Gao et al., 2015; Gokani et al., 2022; Onsager et al., 2007; Yuan & Zong, 2013). Based on superposed epoch analysis of high-speed stream (HSS) driven storms, the study by Borovsky and Denton (2010) suggested that magnetopause shadowing could be crucial for relativistic electron dropouts during HSS storms. Similarly, Meredith et al. (2011) also investigated energetic electron precipitation during HSS storms, showing a strong magnetic local time (MLT) dependence. Moreover, their results suggested that electron precipitation at energies >30 keV are driven by chorus waves, while the dropouts of relativistic electrons are not caused by precipitation. By examining the characteristics of the energetic electron dropouts under different solar conditions using long term data set of intense storms during the years of 1996–2019, Gokani et al. (2022) suggested the more substantial flux decay with stronger solar wind pressure and speed. However, in contrast to previous studies, their results show that it was either northward IMF B_z before turning southward or rapidly fluctuating IMF B_z are important in producing significant dropouts. While all the studies mentioned above focused on the analysis of dropouts at a specific energy or a wide energy range, the studies by Boynton et al. (2016, 2017) investigated the electron flux dropouts over the energy range of tens of keV to several MeV with a high energy resolution. Their results demonstrated far fewer dropouts over energies of 63–~600 keV compared to those below 63 keV and above ~600 keV. In addition, the magnitude of the dropouts strongly depends on energy, which is much stronger at energies above 1 MeV comparing to lower energies. However, both studies are performed at a specific L-shell. Apart from the above-mentioned statistical studies that are based on electron flux measurements, the study of Xiang et al. (2018) investigated the statistical distributions of dropouts over a wide range of μ, K, and L* (the three adiabatic invariants) using electron phase space density (PSD) in adiabatic invariant coordinate and their correlation with various indices, including Dst, IMF B_z, P_{sw}, magnetopause location, and last closed drift shell. Their statistical results suggested that EMIC waves dominate the dropouts at low L* region, which requires the most active geomagnetic and solar wind conditions. However, both EMIC wave scattering and outward radial diffusion associated with magnetopause shadowing contribute to dropouts at high L* region. One of the advantages of analyzing electron PSD is that the adiabatic variations in the observed electron fluxes can be removed. However, this method still requires sophisticated calculations, the assumption of a certain magnetic field model, and a large amount of interpolation, which is computationally expensive compared to the analysis based on electron fluxes. Moreover, since the generations of both chorus and EMIC waves that play an important role in dropouts are strongly associated with substorm injections, whose correlation with dropouts is also important to understand the physical processes of the dropouts, which was not included in their study. Meanwhile, since their study was based on fluxes measured by Magnetic Electron Ion Spectrometer (Blake et al., 2013) and Relativistic Electron Proton Telescope (Baker et al., 2013, 2021) onboard Van Allen Probes, they statistics were confined with energies above ~30 keV. Therefore, there is still a lack of a study that systematically and comprehensively investigates the statistical distribution of electron flux dropouts over the entire outer belt and their dependence on energy, and potential driving parameters including various geomagnetic indices, and solar wind parameters.

In the current study, we comprehensively analyze the statistical morphology of the outer belt electron flux dropouts over energies of 1 keV–10 MeV during storm events using 5-year of observations from Van Allen Probes. Our study, for the first time, systematically analyzes the dependence of dropouts of outer belt electrons over a broad energy and L-shell range on various driving parameters, including IMF B_z, P_{SW}, SYM-H, and AE. In this way, we attempt to diagnose the critical solar drivers and geomagnetic conditions that are responsible for significant electron flux dropouts at different energies, which is crucial for understanding of the underlying physical mechanisms that control the outer belt electron dynamics and future radiation belt forecasts.

The paper is organized as follows. Section 2 describes the database and the criteria to select the dropouts. In Section 3, we comprehensively investigate the statistical distribution of the dropouts and their dependence on energy, L-shell, and various driving parameters. Sections 4 and 5 contain the discussion and conclusions.

2. Data and Methodology

The Energetic Particle Composition and Thermal Plasma suite (ECT; Spence et al., 2013) onboard the twin Van Allen Probes (Mauk et al., 2013) provides high-quality electron flux measurements. The spin-averaged cross-calibrated fitted electron flux data product with high energy resolution is adopted in this study (Boyd et al., 2019). We use TS04D magnetic field model to obtain the McIlwain L-shell (Tsyganenko & Sitnov, 2005). We adopt the measurements of geomagnetic storm index (SYM-H), substorm index (AE), solar wind dynamic pressure (P_{SW}), and IMF B_z provided by OMNIWeb with a time resolution of 1 min.

To systematically examine the statistical distributions of electron flux dropouts during geomagnetic storm events, we perform a superposed epoch analysis of electron fluxes during all storm events when the minimum value of the SYM-H index ($(SYM\text{-}H)_{min}$) extended below −50 nT from 2013 to 2017. Here, the time of epoch time $t = 0$ corresponds to $(SYM\text{-}H)_{min}$. There were 110 storm events selected in this study, which are the same as those in Hua, Bortnik, Chu, et al. (2022) and Hua, Bortnik, Spence, and Reeves (2023). Similar to previous studies (Boynton et al., 2016, 2017), the dropouts are automatically selected based on the following steps and criteria:

1. We first bin the electron fluxes into the grids of 0.1 L × 6 hr UT in four different MLT regions: 00–06, 06–12, 12–18, and 18–24. Here, the averaged absolute fluxes are adopted in each bin. Since Van Allen Probes had a highly elliptical orbit period of ∼9 hr, the time bin size of 6 hr here ensures at least one available measurement in each bin for the most of the time. This bin size has also been widely adopted to investigate the outer belt electron dynamics in previous studies (e.g., Drozdov et al., 2019; Hua, Bortnik, Spence, & Reeves, 2023; Hua et al., 2019; Turner et al., 2015).
2. A decrease of flux by a factor >4 in 6 hr (the electron flux in the previous time step, $j(t-1)$, being at least 4 times larger than the current one, $j(t)$, that is, $\frac{j(t-1)}{j(t)} \geq 4$), or a decrease by a factor >4 in 12 hr while the flux decay by at least a factor of 1.5 in previous two successive time steps ($\frac{j(t-2)}{j(t)} \geq 4$, $\frac{j(t-2)}{j(t-1)} \geq 1.5$, and $\frac{j(t-1)}{j(t)} \geq 1.5$).

   Here, the flux decrease factor is adapted from the studies of Boynton et al. (2016, 2017). For reader's reference, the comparison of the electron flux dropout identification criteria between the current study and the previous statistical studies are listed in Table S1 in Supporting Information S1.
3. We discard data points of identified dropouts if the dropouts are identified for less than five energy channels or less than 3 L-shell bins in the same time bin. We would like to emphasize that our statistics is based on the combined electron flux data with 127 energy channels logarithmically spaced between 10 eV and 20 MeV, which means 20 energy values per decade (Boyd et al., 2019). Therefore, the threshold of 5 energy channels comparing to 20 energy values per decade is still sufficiently small so that Criterion (3) only eliminates data that is too isolated, while the dropouts over a wider energy and spatial range are included in our data set, which are also the dropouts that matter the most and we care the most.

We present two storm events in Figure 1 below as typical examples shown to demonstrate that our selection criteria can successfully identify the dropouts.

Figures 1a–1i present examples of identified dropouts observed by Van Allen Probes at the afternoon sector 12–18 MLT during the 9 October 2013 storm. This is a significant dropout event primarily caused by magnetopause shadowing, and accompanied by outward radial diffusion when the dayside magnetopause was compressed due to the coronal mass ejection (CME)-shock (Foster et al., 2015; Hudson et al., 2015; Paral et al., 2015; Pierrard et al., 2021). A substantial increase in P_{SW} (Figure 1a) accompanied by a reversal of IMF B_z (Figure 1b) just before

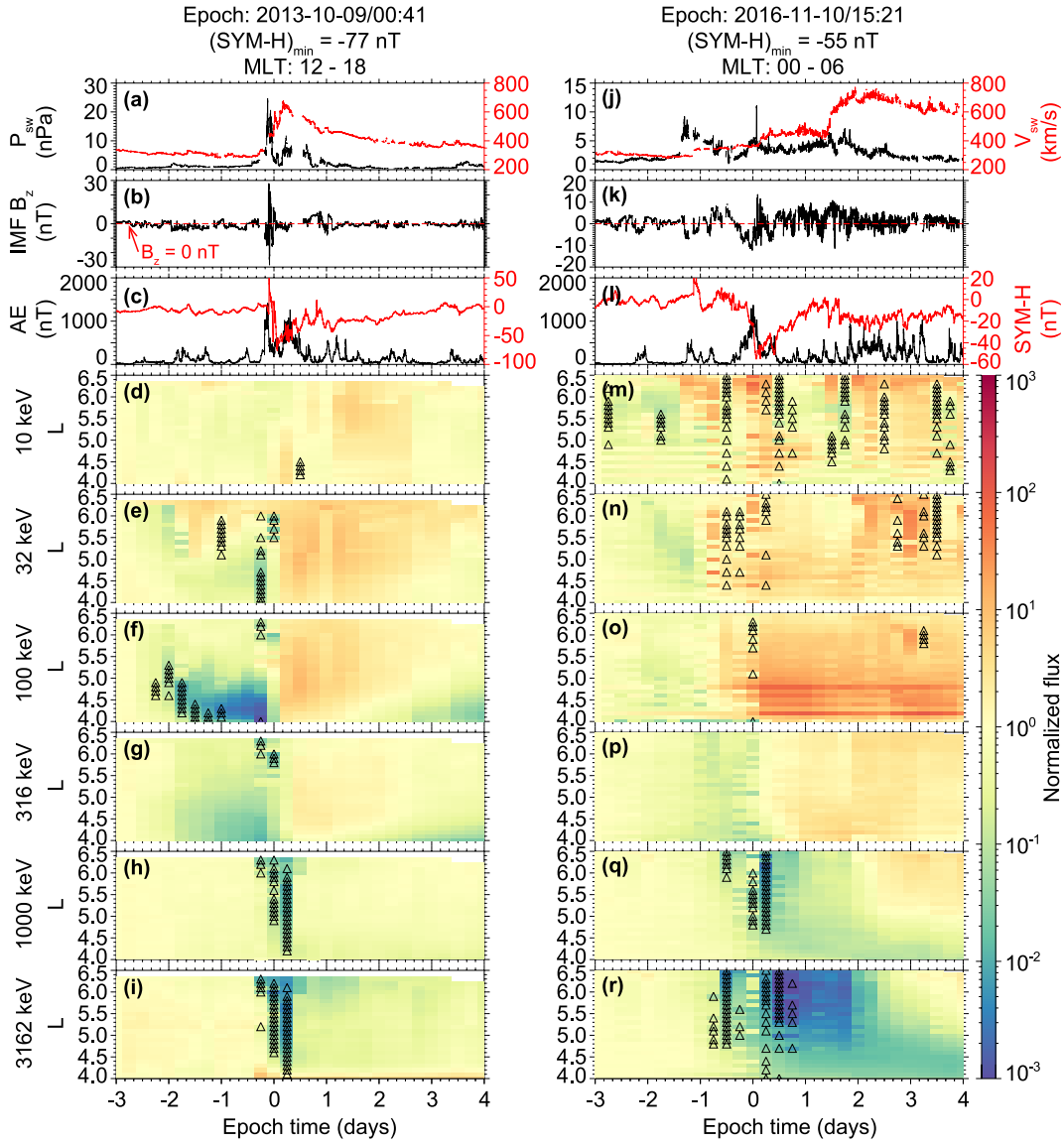

Figure 1. Examples of electron flux dropouts observed by Van Allen Probes during (a–i) the 9 October 2013 storm and (j–r) the 10 November 2016 storm. (a) Solar wind dynamic pressure P_{SW} (black) and speed V_{sw} (red). (b) North-south component of the interplanetary magnetic field (IMF B_z) in Geocentric Solar Magnetospheric (GSM) coordinate. (c) AE (black) and SYM-H (red) indices. (d–i) Superposed epoch analysis of spin-averaged electron fluxes measured by ECT from both Van Allen Probes normalized by the fluxes at $t_{epoch} = -3$ days at 10, 32, 100, 316, 1,000, and 3,162 keV, respectively. Here, the time of $(SYM\text{-}H)_{min}$ is taken as the epoch 0. The identified dropouts are marked as triangles. (j–r) Similar to (a–i) but for the 10 November 2016 storm.

$t_{epoch} \sim 0$ days indicates that there was a strong compression of the magnetopause and potential magnetopause reconnection, which are closely related to the intense storm and substorm activities occurring in the following day (Figure 1c). Figures 1d–1i show the superposed epoch analysis of electron flux evolution observed by both Van Allen Probes normalized by the fluxes at $t_{epoch} = -3$ days at 10, 32, 100, 316, 1,000, and 3,162 keV, respectively. The identified dropouts are marked as triangles. Electron fluxes at 10–100s keV exhibit similar behavior, showing a decrease during the pre-initial phase of the storm and enhancements during the recovery phase that exceed the pre-initial phase of the storm. In particular, the quick electron losses for more than two orders of magnitude at 100 keV were only observed locally close to the heart of the outer belt over $L = \sim 4.0$–5.0, which can be caused by the pitch angle scattering via locally interacting with chorus waves (Bortnik & Thorne, 2007; Hua, Bortnik, & Ma, 2022). In contrast, the sudden and significant electron flux decrease, that is, dropouts, for relativistic electron

fluxes at ≥1 MeV were observed almost over the entire outer belt corresponding to the solar wind dynamic pressure pulse, without showing a clear L-shell dependence. This characteristic of electron flux dropouts is consistent with the strong electron loss to the magnetopause as suggested from the previous studies (Hudson et al., 2015; Paral et al., 2015; Pierrard et al., 2021).

Similarly, examples of electron flux dropouts during the 10 November 2016 storm observed over the dawn sector 00–06 MLT are shown in Figures 1j–1l. In contrast to the 9 October 2013 storm event where the strong substorm activities only lasted about 1 day after reaching $(SYM\text{-}H)_{min}$, the strong substorm activities continued for several days during the recovery phase of the 10 November 2016 storm, as suggested by several spikes in the AE index. Consequently, there are more electron injections and potentially stronger chorus wave activity under such intense and continuous substorms (Hua, Bortnik, Spence, & Reeves, 2023). Since the most efficient energy range of pitch angle scattering of electrons due to chorus waves is from tens to ∼100 keV, with the typical loss time scale varying from tens of minutes to hours (Hua, Bortnik, & Ma, 2022; Ni et al., 2016), the quick electron loss at tens of keV as marked by the triangles could be driven by locally interacting with chorus waves. Although the electron fluxes at hundreds of keV (Figures 1o–1p) decreased modestly during the pre-initial phase of the storm, these electrons quickly recovered during the main phase and recovery phase of the storm, which could be evidence of either rapid acceleration, the Dst effect, or essentially no change in fluxes at these energies. Therefore, the flux decrease of these electrons was not substantial enough to be identified as dropouts. On the contrary, the relativistic electron fluxes significantly decreased by more than two orders of magnitude at $L > \sim 4.5$, with stronger flux decreased observed at higher L-shell compared to the lower L-shell region. Consistent with previous studies (Boynton et al., 2016, 2017), the magnitude of the relativistic electron flux dropouts is much more significant than the electrons at tens of keV. Moreover, these electron flux dropouts were strongly associated with the sudden increase of P_{SW} (Figure 1j) and IMF B_z southward turning (Figure 1k), suggesting a strong impact of magnetopause shadowing. For readers' reference, Figure S1 in Supporting Information S1 presents an example of the superposed epoch analysis of the energy spectra of electron fluxes at a fixed L-shell, which again confirms that our criteria can successfully select the significant and fast dropouts.

3. Statistical Dependence of Dropouts

3.1. Dependence on Electron Energy

Figure 2 shows the statistical electron flux dropout properties as a function of L-shell and electron energy based on both Van Allen Probes observations during the selected 110 storm events. The electron flux dropout sample numbers are shown in Figure 2a. Here, one data sample corresponds to one triangle symbol as shown in Figure 1. Clearly, electron flux dropouts strongly depend on energy. While electron flux dropouts can be frequently observed at energies below ∼100 keV and above ∼1 MeV, the number of dropout samples is extremely small for the medium-energy electrons at hundreds of keV. Figure 2b shows the satellite dwell time for both Van Allen Probes regardless of identification of dropouts, which demonstrates that Van Allen Probes have sufficient coverage over energies of 1 keV–∼6 MeV and L-shells in the outer radiation belt. Figure 2c presents the occurrence rate of the dropouts during storm times, that is, the number of dropout samples divided by the number of satellite dwell time. Electron flux dropouts below ∼100 keV and above ∼1 MeV have larger occurrence rates compared to the medium-energy electrons. The occurrence of the dropouts below 100 keV increases with increasing L-shell at $L < \sim 5.0$ and roughly remains constant at $L = 5.5$–6.5. One of the possible explanations is that chorus wave intensity roughly increases with increasing L-shell at $L = 4.0$–∼6.0 (Meredith et al., 2020). Meanwhile, injected electrons are more likely to penetrate to higher L-shells comparing to the lower L-shells, which can be further lost due to interacting with intense chorus waves. Consequently, the dropout occurrence increases with increasing L-shell at $L < \sim 5.5$. However, more injections at higher L-shell may interrupt the loss processes, possibly resulting in the constant occurrence rate at $L = 5.5$–6.5. In contrast, the occurrence of the dropouts above ∼1 MeV increases with increasing L-shell and extends to lower energies, possibly due to the reasons that the relativistic electrons are more likely to be lost outside the magnetopause by magnetopause shadowing or/and accompanied by the outward radial diffusion, and drift shell splitting at higher L-shells compared to the lower region. In addition, the most efficient energies of relativistic electron pitch-angle diffusion driven by EMIC waves decrease with increasing L-shell (Ni et al., 2015), which can also contribute to higher occurrence rate of dropouts with increasing L-shell and decreasing energy. Furthermore, higher occurrence rate of dropouts at the higher L-shells might also be attributed to more efficient pitch-angle scattering caused by current sheet scattering (Sergeev & Tsyganenko, 1982).

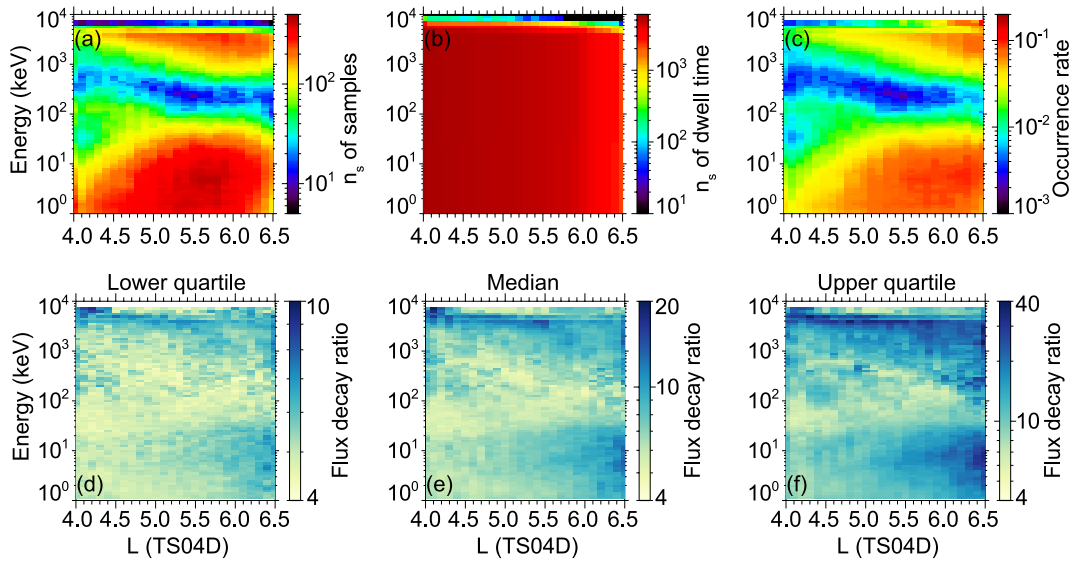

Figure 2. Statistical electron flux dropout properties shown as a function of L-shell and electron energy based on both Van Allen Probes observations during all the geomagnetic storms with $(SYM\text{-}H)_{min}$ below −50 nT during the years 2013–2017. (a) Number of dropout samples. (b) Number of data points for dwell time of both Van Allen Probes. (c) Occurrence rate of electron flux dropouts. (d–f) Lower quartile, median, and upper quartile of the flux decay ratio for the identified dropout events, respectively.

To investigate the magnitude of the electron flux dropouts, we calculate the flux decay ratio for each identified dropout samples, which is the larger one between $\frac{j(t-1)}{j(t)}$ and $\frac{j(t-2)}{j(t)}$. Figures 2d–2f show the lower quartile, median, and the upper quartile of the flux decay ratio for the identified dropout events, respectively. Similar to the occurrence rate of the dropouts, the magnitude of the dropouts is larger for electrons below ∼100 keV and above ∼1 MeV comparing to the medium-energy electrons at hundreds of keV, with more significant dropouts extending to hundreds of keV with increasing L-shell. In addition, the flux decay ratio is overall larger at energies above ∼1 MeV comparing to those below ∼100 keV. Both the occurrence rate and flux decay ratio at all energies increase with increasing L-shell, which expands to medium-energy electrons, suggesting that magnetopause shadowing accompanied by outward radial diffusion can contribute significantly to the dropouts at $L >$ ∼6.0. Nevertheless, the sudden decrease in both occurrence rate and the flux decay ratio at medium-energy suggests that apart from outward radial diffusion, other mechanisms are needed to cause the outer belt electron dropouts.

3.2. Dependence on IMF B_z

To determine the impact of IMF B_z on the electron flux dropouts, we separate the events into northward and southward IMF B_z conditions. In this study, the southward (northward) IMF B_z condition is determined by the ratio of the time-integrated absolute value of southward IMF B_z to that of northward IMF B_z larger (smaller) than 1 during the previous 3 hr time interval of the identified dropout sample. Figure 3 shows the occurrence rate of electron flux dropouts at various MLT sectors, from left to right: 00–06, 06–12, 12–18, and 18–24 under (panels a to d) northward and (panels e to h) southward IMF B_z conditions, respectively. The median results of the flux decay ratio for the identified dropout events at indicated MLT sector during northward and southward IMF B_z condition are also presented in the lower panels of Figure 3. Interestingly, the electron flux dropouts at energies below ∼100 keV have higher occurrence rate during northward IMF B_z conditions compared to the southward IMF B_z conditions, while there is no significant difference of the flux decay ratio under different IMF B_z conditions. These electron flux dropouts also strongly depend on MLT, showing a much higher occurrence rate with peak reaching >0.1 on the nightside over 18–06 MLT compared to the dayside. In particular, the dusk side (12–18 MLT) exhibits the lowest occurrence rate of dropouts for electrons below ∼100 keV. According to previous statistics (Li et al., 2016; Meredith et al., 2020), chorus waves typically have larger wave amplitude on the nightside, with the weakest intensity over the dusk side. The consistency of the MLT dependence of electron flux dropouts at energies below ∼100 keV and chorus wave intensity suggests that chorus waves play an essential

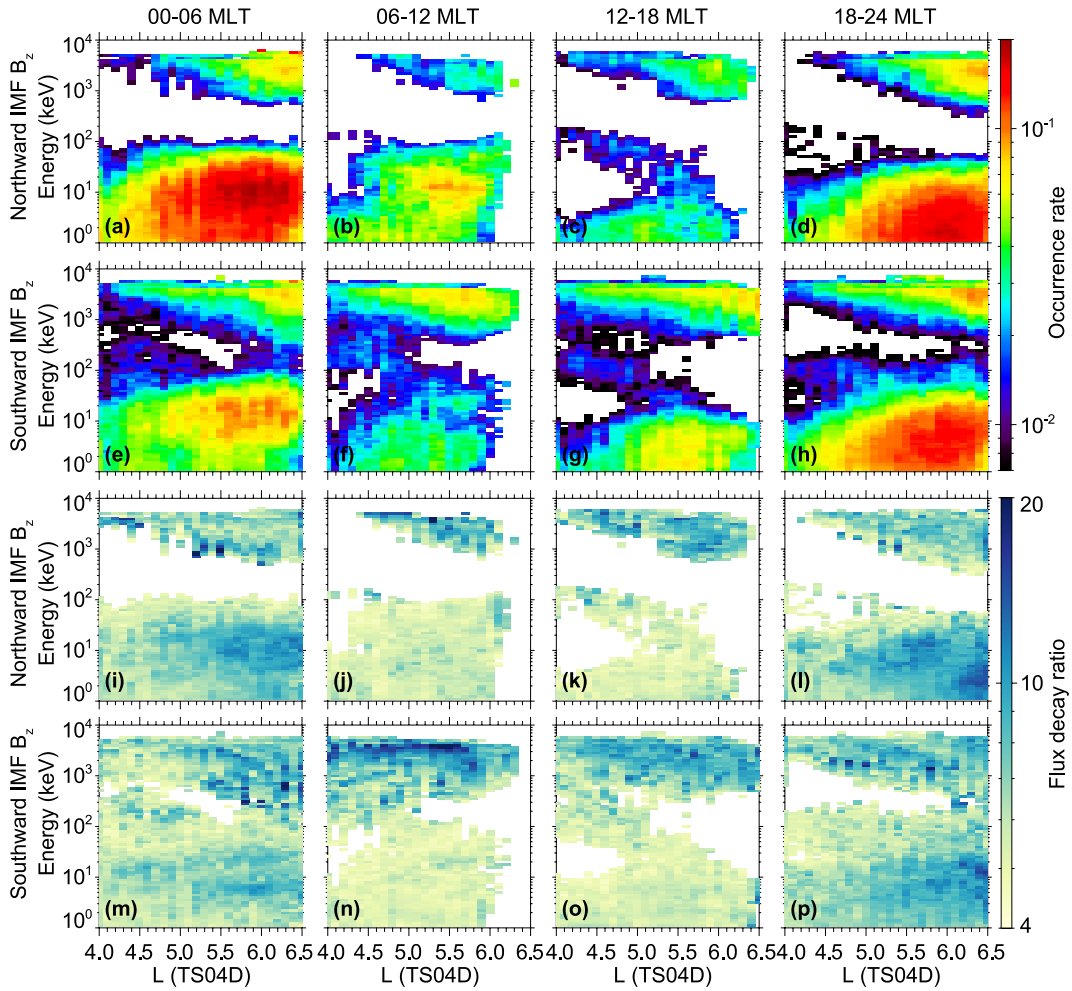

Figure 3. Occurrence rate of electron flux dropouts at various magnetic local time (MLT) sectors, from left to right: 00–06, 06–12, 12–18, and 18–24 during (a–d) northward and (e–h) southward interplanetary magnetic field (IMF) B_z conditions, respectively. Median results of the flux decay ratio for the identified dropout events at indicated MLT sectors during (i–l) northward and (m–p) southward IMF B_z conditions, respectively.

role in causing the dropouts of electrons below ~100 keV. In contrast, the dropouts above ~1 MeV demonstrate higher occurrence rate and stronger flux decay ratio under the southward IMF B_z conditions compared to the northward conditions. Although the occurrence rate of the dropouts for relativistic electrons does not show clear dependence on MLT, these electron flux dropouts have slightly stronger flux decay ratio on the dayside (06–18 MLT) compared to the nightside (18–06 MLT).

3.3. Dependence on P_{SW}

Similar to Figure 3, Figure 4 shows the statistical distributions of electron flux dropouts during weak and strong P_{SW} conditions. Here, the strong P_{SW} condition is defined as mean(P_{SW}) > 2 nPa, where the mean(P_{SW}) is the mean profile of the P_{SW} during the previous 3 hr time interval of the identified dropout sample. Apart from the higher occurrence of dropouts of electrons below ~100 keV over 18–24 MLT during strong P_{SW} conditions (Figure 4h), there is no clear dependence of occurrence rate of dropouts of these low-energy electrons on various P_{SW} conditions (Figures 4a–4h). Nevertheless, the dropouts of these low-energy electrons exhibit stronger flux decay ratio during strong P_{SW} conditions compared to weak P_{SW} conditions (Figurse 4i–4p).

In contrast, P_{SW} conditions significantly influence the dropouts of relativistic electrons above ~1 MeV, with majority of the significant dropouts observed during strong P_{SW} conditions. The relativistic electron flux dropouts barely occur during weak P_{SW} conditions, indicating that most of the dropouts of the relativistic electrons

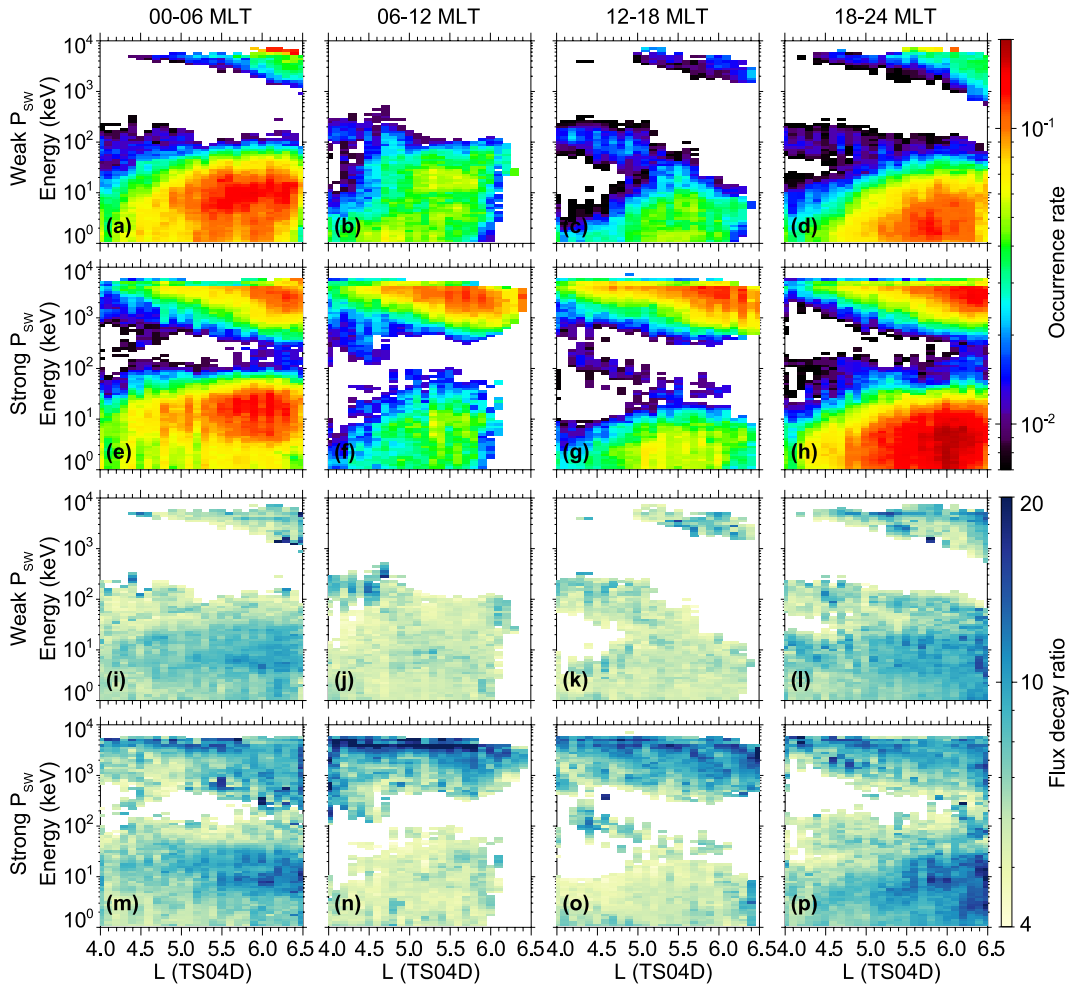

Figure 4. Same format as Figure 3 but for results during (a–d and i–l) weak and (e–h and m–p) strong P_{SW} conditions.

are associated with the compression of the magnetopause caused by the strong P_{SW}, supporting the crucial role of magnetopause shadowing in causing these electron dropouts. In addition, the strongest dropouts with flux decay ratio reaching ~20 are found at multi-MeV during strong P_{SW} condition on the dayside, especially at the 06–12 MLT, which is close to the peak of the flux decay ratio during southward IMF B_z condition (Figure 3n). These electron dropouts can be caused by the combined impacts of southward IMF B_z and strong P_{SW} conditions when both compression of magnetopause and outward radial diffusion get enhanced. Meanwhile, the sudden increase in solar wind pressure pulses can also enhance the temperature anisotropic distributions of ions and electrons, leading to excitation of both EMIC and chorus waves on the dayside that can contribute to electron loss (McCollough et al., 2010; Tsurutani et al., 2016; Zhang et al., 2017). The increase of dropout occurrence rates on the nightside with increasing P_{SW} might be attributed to the stretching of the magnetic field line in the tail region during strong P_{SW} conditions, causing the electrons moving adiabatically to lower energies or higher L-shells.

3.4. Dependence on SYM-H

To examine the impact of the ring current buildup during geomagnetic storms on electron flux dropouts, Figure 5 displays the statistical distributions of dropouts during weak and strong SYM-H conditions. We define the strong SYM-H condition as the mean(SYM-H) < −30 nT, where the mean(SYM-H) is the mean profile of the SYM-H during the previous 3 hr time interval of the identified dropout sample. Overall, the dropouts of electrons at all energies have higher occurrence rate and stronger flux decay ratio during strong SYM-H conditions compared to weak SYM-H conditions. Since the geomagnetic storms are strongly correlated with the strong solar wind activity and southward IMF B_z conditions, the more significant electron dropouts are more likely to be observed

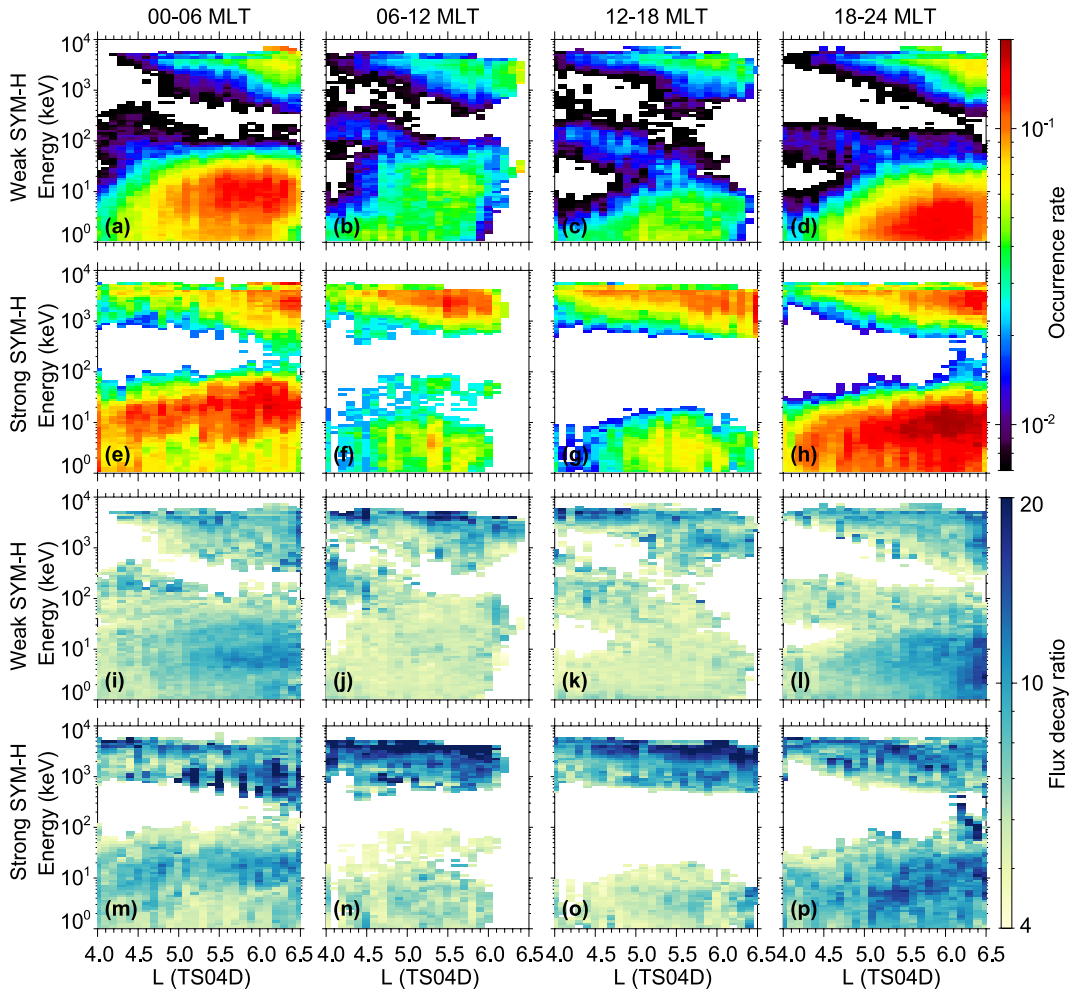

Figure 5. Same format as Figure 3 but for results during (a–d and i–l) weak and (e–h and m–p) strong SYM-H conditions.

during active times compared to quiet conditions. Furthermore, the stronger and more frequently occurring dropouts during strong SYM-H conditions compared to the weak one may be attributed to the adiabatic electron loss due to Dst effect when the ring current increases, which serves to move electrons outward to larger L-shells due to an enhancement in the ring current (Kim & Chan, 1997), and act in concert with magnetopause shadowing. Since different geomagnetic indices and solar wind parameters are intrinsically correlated with each other, it is difficult to distinguish the contributions of the Dst effect to the electron dropouts from other loss mechanisms. Nevertheless, as discussed in the study of Boynton et al. (2016), much higher occurrence and flux decay ratio of dropouts at lower and higher energies compared to the intermediate energies suggests that the Dst effect does not dominantly cause these dropouts.

3.5. Dependence on AE

To examine the impact of substorms on electron flux dropouts, Figure 6 presents the dropout events sorted according to weak and strong AE conditions. Here, the strong AE condition is defined as mean(AE) > 100 nT, where the mean(AE) is the mean profile of the AE during the previous 3 hr time interval of the identified dropout sample. Surprisingly, the occurrence rate of the electron flux dropouts below ∼100 keV is higher during weak AE conditions at 00–06 MLT, which is different from our speculation that more intense chorus wave on the nightside during strong AE condition can drive more frequent dropouts of electrons below ∼100 keV.

The reason may be that the more frequent and intense electron injections and enhanced inward radial diffusion during strong AE conditions can refill electron fluxes even as they are being simultaneously precipitated to the

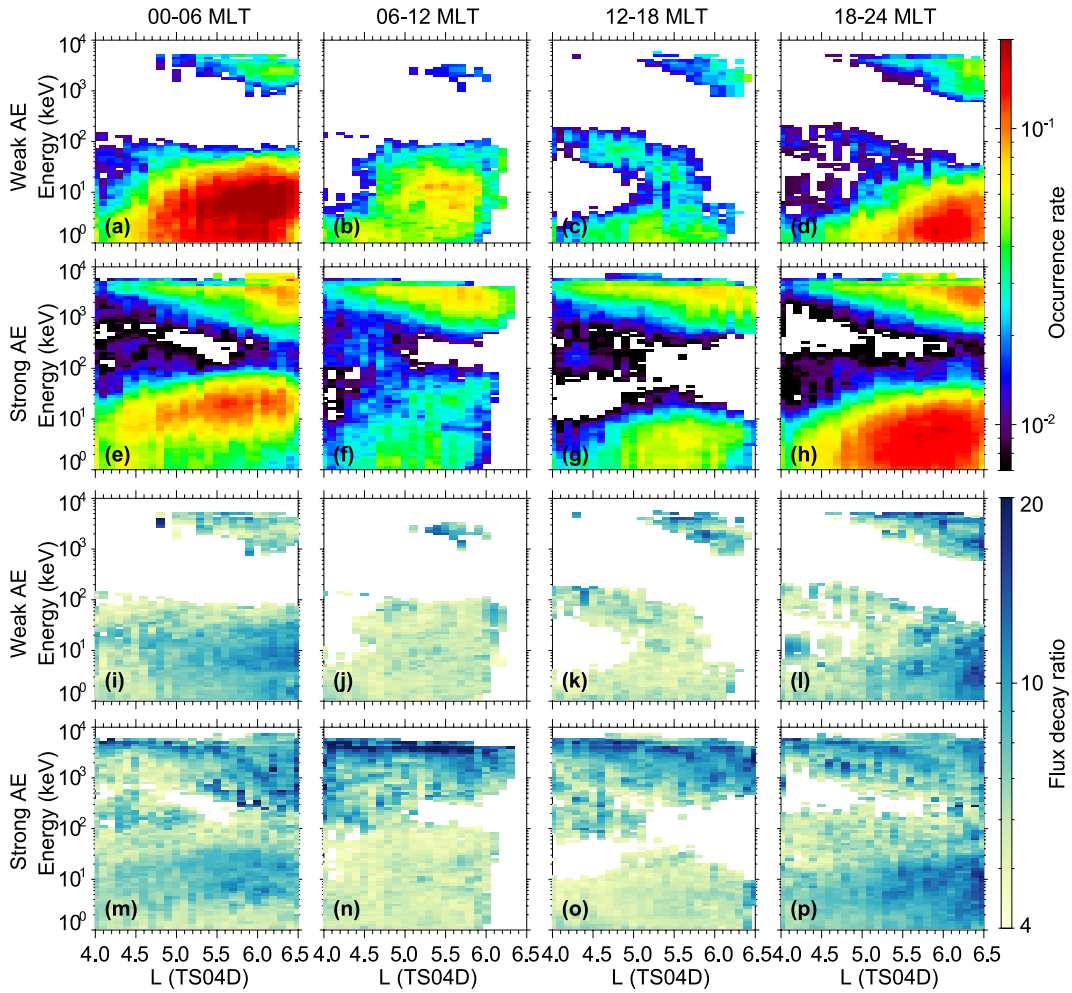

Figure 6. Same format as Figure 3 but for results during (a–d and i–l) weak and (e–h and m–p) strong AE conditions.

atmosphere, and thus interrupt the loss processes caused by wave-particle interactions due to chorus waves. Therefore, overly active substorm conditions are not favorable for the electron flux dropouts below ~100 keV at 00–06 MLT. In addition, the flux decay ratio of these low energy electrons is similar under different AE conditions. In contrast, dropouts of electron fluxes above ~1 MeV show higher occurrence rate and stronger flux decay ratio during strong AE conditions compared to weak AE conditions. Although the injected ions during strong AE conditions can provide free energy for the generation of EMIC waves that can effectively cause relativistic electron flux dropouts, it is difficult to isolate the individual role of substorms on dropouts as AE index is strongly correlated with SYM-H and solar wind drivers.

4. Discussion

The present statistical analysis of electron flux dropouts is unique in a number of ways. Here we analyze: (a) the global morphology of the statistical distribution of the dropouts as a function of energy, spanning from 1 keV to 10 MeV, and L-shell spanning over L = 4.0–6.5; (b) dependence of dropouts on MLT, and (c) various driving parameters, including IMF B_z, P_{SW}, SYM-H, and AE indices.

Figure 7 presents a schematic illustration summarizing our findings, and listing the possible driving parameters for electron flux dropouts at different L-shells and electron energies in the outer radiation belt. The dropouts are naturally divided into three different regions. First, Region a, corresponding to the relativistic electron flux dropouts at energies above ~1 MeV, demonstrates high occurrence rate during southward B_z, strong P_{SW}, SYM-H and AE conditions, and having no clear dependence on MLT. In addition, the large flux decay ratio in Region a is

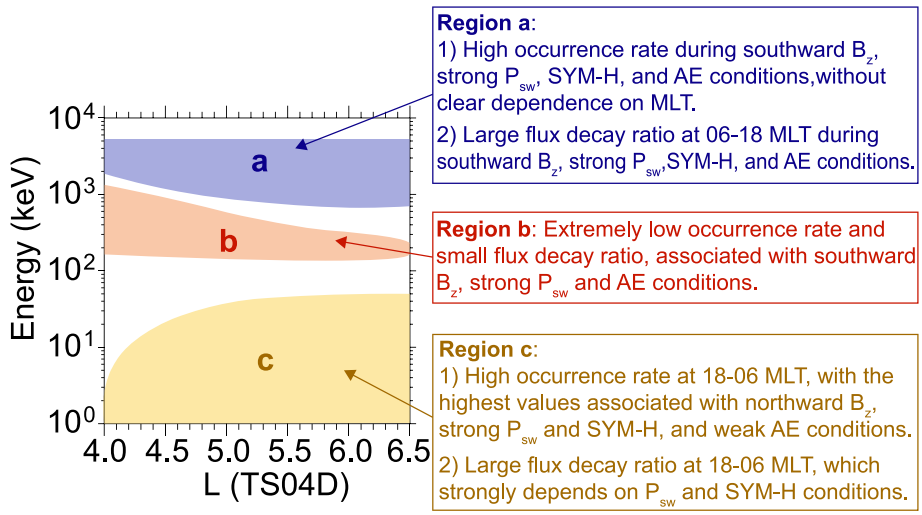

Figure 7. Schematic illustration of possible driving parameters for electron flux dropouts at different L-shells and electron energies in the Earth's outer radiation belt.

found on the dayside (06–18 MLT), which strongly correlated with southward IMF B_z, strong P_{SW}, SYM-H and AE conditions. Therefore, significant relativistic electron flux dropouts preferentially occur during active solar wind drivers and geomagnetic conditions, which can be the result of the combined impact of the magnetopause shadowing accompanied by outward transport due to the Dst effect, radial diffusion, and precipitation via locally interacting with EMIC waves. Second, Region b is characterized by the extremely low occurrence rate and small flux decay ratio for medium-energy electrons at hundreds of keV, and is associated with the southward IMF B_z, strong P_{SW} and AE conditions, indicating that the dropouts of these electrons are rare and only occur during extremely active times. Another possible explanation is that these electrons can be easily accelerated by chorus waves or/and enhanced inward radial diffusion with a typical time scale of several hours during the main phase of the storm (Hua, Bortnik, & Ma, 2022), which is shorter than those electron acceleration at >∼1 MeV that takes tens of hours to days during the recovery phase of the storm (Hua, Bortnik, & Ma, 2022; Thorne et al., 2013). Since our statistics are based on the electron fluxes binned into the grids of 0.1 L × 6 hr UT, significant flux decay followed by quick flux enhancement within 6 hr could in principle occur, which would mask a dropout in these energies and prevent them from being identified as dropouts in this study. While that is a possibility, we should expect to see at least some small decrease in the 100s keV electron fluxes, reflecting the probability that the electron dropout would statistically occur uniformly throughout the 6-hr time bin and thus may not always be fully compensated by a rapid acceleration. Moreover, the few 100 keV energy has been shown in previous studies (e.g., Summers et al., 2002) to be a "pivotal" energy, below which electron fluxes decrease and give up their energy to grow waves, and above which electron fluxes increase at relativistic energies, causing enhancements of relativistic electrons. So it may indeed be the case that 100s keV electrons experience very few dropouts as these electrons can be quickly accelerated and reach the saturation state (Hua, Bortnik, & Ma, 2022).

The electron flux dropouts below ∼100 keV in Region c demonstrate strong MLT dependence, which have high occurrence rate at nightside (18–06 MLT), with the highest occurrence rate associated with the northward IMF B_z, strong P_{SW} and SYM-H, and weak AE conditions. The largest flux decay ratio in this region is found at night-side, with strongly depends on P_{SW} and SYM-H conditions. Nevertheless, the dominant loss mechanism for the fewer dropouts on the dayside is also important, for example, their correlations with chorus wave activities and substorm injections, which deserves more investigation in the future study.

Although we separately analyze the dependence of dropouts on various driving parameters, including IMF B_z, P_{SW}, SYM-H, and AE, it is still difficult to differentiate the distinct role of different driving parameters in causing electron flux dropouts since these parameters are intrinsically correlated with each other. Future study can employ machine learning (ML) technique, such as explainable ML technique, to quantitatively analyze the attribution of various driving parameters on producing dropouts and potentially unravel the underlying physical processes (Ma et al., 2023). In addition, although the current study specifically focuses on investigation of dropouts during storm

events, understanding the statistical properties of the non-storm time dropouts are also significant and interesting, which will be left to the future study. It is noteworthy that there are still some uncertainties about the definitions of the "strong" and "weak" conditions for various driving parameters, that is, IMF B_z, P_{SW}, SYM-H, and AE in the present study. To check the sensitivity on these definitions, we also tried to use different threshold, instantaneous extreme values (e.g., max(P_{SW}), min(SYM-H)) and mean values calculated in the different time intervals (e.g., previous 3 and 6 hr of the identified dropout sample), which all gives similar conclusions. Moreover, our major conclusions do not heavily depend on the selection criteria. For example, the statistical properties of the dropouts have similar distributions with a smaller flux bin size in time domain. Removing Criterion (3) or slightly adjusting the flux decrease threshold in Criterion (2), the statistical distributions of dropouts remain similar. Considering that the identification criteria vary in many previous studies (see Table S1 in Supporting Information S1), it is an important research topic itself of understanding how the uncertainties in the choice of the identification criteria influence the statistical properties of the dropouts. Furthermore, since the results of these statistical distributions of dropouts can serve as training data set to predict the dropouts using ML technique (Bortnik et al., 2018), it is of great significance to quantitatively analyze the sensitivity of the statistical properties of the dropouts to various identification criteria, which will be left to a follow-up study in the future.

5. Conclusions

In the current study, we comprehensively investigated the statistical distribution of the outer belt electron flux dropouts as a function of energy spanning from 1 keV to 10 MeV at L-shell over the range 4.0–6.5 during geomagnetic storms using 5-year observations from Van Allen Probes. Our study systematically analyzes the dependence of dropouts of outer belt electrons over a broad energy and L-shell range on various driving parameters, including IMF B_z, P_{SW}, SYM-H, and AE. In this way, we attempt to identify the critical solar wind driver and geomagnetic conditions that cause significant electron flux dropouts at different energies, which is crucial for understanding of the underlying physical mechanisms that control the outer belt electron dynamics and future radiation belt forecast. Our major conclusions are as follows:

1. Electron flux dropouts strongly depends on electron energies, naturally dividing into three distinct regions at energies above ∼1 MeV (Region a), below ∼100 keV (Region c) and much smaller occurrence rate at medium-energies around hundreds of keV (Region b). The flux decay ratio is higher at energies above ∼1 MeV compared to the energies below ∼100 keV.
2. There is no clear MLT dependence of occurrence rate of relativistic electron flux dropouts above ∼1 MeV, but the flux decay ratio of these dropouts is more significant on the dayside, with stronger decay associated with southward IMF B_z, strong P_{SW}, SYM-H, and AE conditions.
3. The flux dropouts of electrons below ∼100 keV strongly depend on MLT, consistent with their slower (∼hour) drift periods. This dependence has high occurrence rate at the nightside (18–06 MLT), with the highest occurrence rate associated with northward B_z, strong P_{SW} and SYM-H, and weak AE conditions. The strongest flux decay of these dropouts is found on nightside, which strongly depends on P_{SW} and SYM-H conditions.

While the precise causality of these dropouts is yet to be fully determined, the strong dependence on P_{SW} and SYM-H are suggestive of magnetopause shadowing, whereas SYM-H, AE and southward B_z would point to wave-driven losses.

Data Availability Statement

The Van Allen probes ECT data are publicly available https://rbsp-ect.newmexicoconsortium.org/data_pub/. The geomagnetic indices are available from the OMNIWeb (https://omniweb.gsfc.nasa.gov/ow_min.html). The data used to produce figures in the current study can be retrieved at https://doi.org/10.6084/m9.figshare.23576784.v1 (Hua, Bortnik, & Ma, 2023).

Acknowledgments
The authors would like to gratefully thank the Van Allen Probes team, particularly the ECT team for providing the electron flux data. This work was primarily supported by funding from subgrant 1559841 to the University of California, Los Angeles, from the University of Colorado Boulder under NASA Prime Grant agreement 80NSSC20K1580 and NSF GEM awards 2025706 and 2247255.

References

Baker, D. N., Hoxie, V., Zhao, H., Jaynes, A. N., Kanekal, S., Li, X., & Elkington, S. (2019). Multiyear measurements of radiation belt electrons: Acceleration, transport, and loss. *Journal of Geophysical Research: Space Physics*, *124*(4), 2588–2602. https://doi.org/10.1029/2018ja026259

Baker, D. N., Kanekal, S., Blake, J. B., Klecker, B., & Rostoker, G. (1994). Satellite anomalies linked to electron increase in the magnetosphere. *Eos, Transactions American Geophysical Union*, *75*(35), 401–405. https://doi.org/10.1029/94EO01038

Baker, D. N., Kanekal, S. G., Hoxie, V., Li, X., Jaynes, A. N., Zhao, H., et al. (2021). The relativistic electron-proton telescope (REPT) investigation: Design, operational properties, and science highlights. *Space Science Reviews*, *217*(5), 68. https://doi.org/10.1007/s11214-021-00838-3

Baker, D. N., Kanekal, S. G., Hoxie, V. C., Batiste, S., Bolton, M., Li, X., et al. (2013). The relativistic electron-proton telescope (REPT) instrument on board the radiation belt storm probes (RBSP) spacecraft: Characterization of Earth's radiation belt high-energy particle populations. *Space Science Reviews*, *179*(1–4), 337–381. https://doi.org/10.1007/s11214-012-9950-9

Baker, D. N., Kanekal, S. G., Li, X., Monk, S. P., Goldstein, J., & Burch, J. L. (2004). An extreme distortion of the Van Allen belt arising from the "Hallowe'en" solar storm in 2003. *Nature*, *432*(7019), 878–881. https://doi.org/10.1038/nature03116

Blake, J. B., Carranza, P. A., Claudepierre, S. G., Clemmons, J. H., Crain, W. R., Dotan, Y., et al. (2013). The magnetic electron ion spectrometer (MagEIS) instruments aboard the radiation belt storm probes (RBSP) spacecraft. *Space Science Reviews*, *179*(1–4), 383–421. https://doi.org/10.1007/s11214-013-9991-8

Blum, L. W., & Breneman, A. W. (2020). Chapter 3—Observations of radiation belt losses due to cyclotron wave-particle interactions. In *The dynamic loss of Earth's radiation belts*. Elsevier. https://doi.org/10.1016/B978-0-12-813371-2.00003-2

Borovsky, J. E., & Denton, M. H. (2010). Magnetic field at geosynchronous orbit during high-speed stream-driven storms: Connections to the solar wind, the plasmasheet, and the outer electron radiation belt. *Journal of Geophysical Research*, *115*(A8), A08217. https://doi.org/10.1029/2009ja015116

Bortnik, J., Chu, X., Ma, Q., Li, W., Zhang, X., Thorne, R. M., et al. (2018). Artificial neural networks for determining magnetospheric conditions. In E. Camporeale, S. Wing, & J. R. Johnson (Eds.), *Machine learning techniques for space weather, machine learning techniques for space weather* (pp. 279–300). Elsevier Inc. https://doi.org/10.1016/B978-0-12-811788-0.00011-1

Bortnik, J., & Thorne, R. M. (2007). The dual role of ELF/VLF chorus waves in the acceleration and precipitation of radiation belt electrons. *Journal of Atmospheric and Solar-Terrestrial Physics*, *69*(3), 378–386. https://doi.org/10.1016/j.jastp.2006.05.030

Bortnik, J., Thorne, R. M., O'Brien, T. P., Green, J. C., Strangeway, R. J., Shprits, Y. Y., & Baker, D. N. (2006). Observation of two distinct, rapid loss mechanisms during the 20 November 2003 radiation belt dropout event. *Journal of Geophysical Research*, *111*(A12), A12216. https://doi.org/10.1029/2006JA011802

Boyd, A. J., Reeves, G. D., Spence, H. E., Funsten, H. O., Larsen, B. A., Skoug, R. M., et al. (2019). RBSP-ECT combined spin-averaged electron flux data product. *Journal of Geophysical Research: Space Physics*, *124*(11), 9124–9136. https://doi.org/10.1029/2019JA026733

Boynton, R. J., Mourenas, D., & Balikhin, M. A. (2016). Electron flux dropouts at Geostationary Earth Orbit: Occurrences, magnitudes, and main driving factors. *Journal of Geophysical Research: Space Physics*, *121*(9), 8448–8461. https://doi.org/10.1002/2016JA022916

Boynton, R. J., Mourenas, D., & Balikhin, M. A. (2017). Electron flux dropouts at L∼4.2 from Global Positioning System satellites: Occurrences, magnitudes, and main driving factors. *Journal of Geophysical Research: Space Physics*, *122*, 11428–11441. https://doi.org/10.1002/2017JA024523

Capannolo, L., Li, W., Millan, R., Smith, D., Sivadas, N., Sample, J., & Shekhar, S. (2022). Relativistic electron precipitation near midnight: Drivers, distribution, and properties. *Journal of Geophysical Research: Space Physics*, *127*(1), e2021JA030111. https://doi.org/10.1029/2021JA030111

Clilverd, M. A., Rodger, C. J., Andersson, M., Seppälä, A., & Verronen, P. T. (2015). Linkages between the radiation belts, polar atmosphere and climate: Electron precipitation through wave particle interactions. In I. Mann, et al. (Eds.), *Waves, particles and storms in geospace (Chapter 14)*. Oxford University Press.

Delcourt, D. C., Sauvaud, J.-A., Martin, R. F., & Moore, T. E. (1996). On the nonadiabatic precipitation of ions from the near-Earth plasma sheet. *Journal of Geophysical Research*, *101*(A8), 17409–17418. https://doi.org/10.1029/96JA01006

Drozdov, A. Y., Allison, H. J., Shprits, Y. Y., Usanova, M. E., Saikin, A., & Wang, D. (2022). Depletions of multi-MeV electrons and their association to minima in phase space density. *Geophysical Research Letters*, *49*(8), e2021GL097620. https://doi.org/10.1029/2021gl097620

Drozdov, A. Y., Aseev, N., Effenberger, F., Turner, D. L., Saikin, A., & Shprits, Y. Y. (2019). Storm time depletions of multi-MeV radiation belt electrons observed at different pitch angles. *Journal of Geophysical Research: Space Physics*, *108*(11), 1249–8953. https://doi.org/10.1029/2019JA027332

Foster, J. C., Wygant, J. R., Hudson, M. K., Boyd, A. J., Baker, D. N., Erickson, P. J., & Spence, H. E. (2015). Shock-induced prompt relativistic electron acceleration in the inner magnetosphere. *Journal of Geophysical Research: Space Physics*, *120*(3), 1661–1674. https://doi.org/10.1002/2014JA020642

Gao, X., Li, W., Bortnik, J., Thorne, R. M., Lu, Q., Ma, Q., et al. (2015). The effect of different solar wind parameters upon significant relativistic electron flux dropouts in the magnetosphere. *Journal of Geophysical Research: Space Physics*, *120*(6), 4324–4337. https://doi.org/10.1002/2015JA021182

George, H., Reeves, G., Cunningham, G., Kalliokoski, M. M. H., Kilpua, E., Osmane, A., et al. (2022). Contributions to loss across the magnetopause during an electron dropout event. *Journal of Geophysical Research: Space Physics*, *127*(10), e2022JA030751. https://doi.org/10.1029/2022JA030751

Gokani, S. A., Han, D.-S., Selvakumaran, R., & Pant, T. K. (2022). Dependence of radiation belt flux depletions at geostationary orbit on different solar drivers during intense geomagnetic storms. *Frontiers in Astronomy and Space Sciences*, *9*, 952486. https://doi.org/10.3389/fspas.2022.952486

Gray, P. C., & Lee, L. C. (1982). Particle pitch angle diffusion due to nonadiabatic effects in the plasma sheet. *Journal of Geophysical Research*, *87*(A9), 7445–7452. https://doi.org/10.1029/JA087iA09p07445

Green, J. C., Onsager, T. G., O'Brien, T. P., & Baker, D. N. (2004). Testing loss mechanisms capable of rapidly depleting relativistic electron flux in the Earth's outer radiation belt. *Journal of Geophysical Research*, *109*(A12), A12211. https://doi.org/10.1029/2004JA010579

Hua, M., Bortnik, J., Chu, X., Aryan, H., & Ma, Q. (2022). Unraveling the critical geomagnetic conditions controlling the upper limit of electron fluxes in the Earth's outer radiation belt. *Geophysical Research Letters*, *49*(22), e2022GL101096. https://doi.org/10.1029/2022GL101096

Hua, M., Bortnik, J., & Ma, D. (2023). Dependence of electron flux dropouts in the Earth's outer radiation belt on energy and driving parameters during Geomagnetic Storms [Dataset]. Figshare. https://doi.org/10.6084/m9.figshare.23576784.v1

Hua, M., Bortnik, J., & Ma, Q. (2022). Upper limit of outer radiation belt electron acceleration driven by whistler-mode chorus waves. *Geophysical Research Letters*, *49*(15), e2022GL099618. https://doi.org/10.1029/2022GL099618

Hua, M., Bortnik, J., Spence, H. E., & Reeves, G. D. (2023). Testing the key processes that accelerate outer radiation belt relativistic electrons during geomagnetic storms. *Frontiers in Astronomy and Space Science*, *10*, 1168636. https://doi.org/10.3389/fspas.2023.1168636

Hudson, M. K., Paral, J., Kress, B. T., Wiltberger, M., Baker, D. N., Foster, J. C., et al. (2015). Modeling CME-shock-driven storms in 2012–2013: MHD test particle simulations. *Journal of Geophysical Research: Space Physics*, *120*(2), 1168–1181. https://doi.org/10.1002/2014JA020833

Imhof, W. L., Voss, H. D., Mobilia, J., Datlowe, D. W., & Gaines, E. E. (1991). The precipitation of relativistic electrons near the trapping boundary. *Journal of Geophysical Research*, *96*(A4), 5619–5629. https://doi.org/10.1029/90JA02343

Imhof, W. L., Robinson, R. M., Nightingale, R. W., Gaines, E. E., & Vondrak, R. R. (1993). The outer boundary of the Earth's electron radiation belt: Dependence upon L, energy, and equatorial pitch angle. *Journal of Geophysical Research*, *98*(A4), 5925–5934. https://doi.org/10.1029/92JA02553

Kang, S.-B., Fok, M.-C., Komar, C., Glocer, A., Li, W., & Buzulukova, N. (2018). An energetic electron flux dropout due to magnetopause shadowing on 1 June 2013. *Journal of Geophysical Research: Space Physics*, *123*(2), 1178–1190. https://doi.org/10.1002/2017JA024879

Kim, H.-J., & Chan, A. A. (1997). Fully adiabatic changes in storm time relativistic electron fluxes. *Journal of Geophysical Research*, *102*(A10), 22107–22116. https://doi.org/10.1029/97JA01814

Li, W., & Hudson, M. K. (2019). Earth's Van Allen radiation belts: From discovery to the Van Allen Probes era. *Journal of Geophysical Research: Space Physics*, *124*(11), 8319–8351. https://doi.org/10.1029/2018JA025940

Li, W., Santolik, O., Bortnik, J., Thorne, R. M., Kletzing, C. A., Kurth, W. S., & Hospodarsky, G. B. (2016). New chorus wave properties near the equator from Van Allen Probes wave observations. *Geophysical Research Letters*, *43*(10), 4725–4735. https://doi.org/10.1002/2016GL068780

Lyu, X., Ma, Q., Tu, W., Li, W., & Capannolo, L. (2022). Modeling the simultaneous dropout of energetic electrons and protons by EMIC wave scattering. *Geophysical Research Letters*, *49*(20), e2022GL101041. https://doi.org/10.1029/2022GL101041

Ma, D., Bortnik, J., Chu, X., Claudepierre, S. G., Ma, Q., & Kellerman, A. (2023). Opening the black box of the radiation belt machine learning model. *Space Weather*, *21*(4), e2022SW003339. https://doi.org/10.1029/2022SW003339

Ma, X., Xiang, Z., Ni, B. B., Fu, S., Cao, X., Hua, M., et al. (2020). On the loss mechanisms of radiation belt electron dropouts during the 12 September 2014 geomagnetic storm. *Earth and Planetary Physics*, *4*(6), 598–610. https://doi.org/10.26464/epp2020060

Mauk, B. H., Fox, N. J., Kanekal, S. G., Kessel, R. L., Sibeck, D. G., & Ukhorskiy, A. (2013). Science objectives and rationale for the radiation belt storm Probes mission. *Space Science Reviews*, *179*(1–4), 3–27. https://doi.org/10.1007/s11214-012-9908-y

McCollough, J. P., Elkington, S. R., Usanova, M. E., Mann, I. R., Baker, D. N., & Kale, Z. C. (2010). Physical mechanisms of compressional EMIC wave growth. *Journal of Geophysical Research*, *115*(A10), A10214. https://doi.org/10.1029/2010JA015393

Meredith, N. P., Horne, R. B., Glauert, S. A., & Anderson, R. R. (2007). Slot region electron loss timescales due to plasmaspheric hiss and lightning-generated whistlers. *Journal of Geophysical Research*, *112*(A8), A08214. https://doi.org/10.1029/2007JA012413

Meredith, N. P., Horne, R. B., Lam, M. M., Denton, M. H., Borovsky, J. E., & Green, J. C. (2011). Energetic electron precipitation during high-speed solar wind stream driven storms. *Journal of Geophysical Research*, *116*(A5), A05223. https://doi.org/10.1029/2010ja016293

Meredith, N. P., Horne, R. B., Shen, X.-C., Li, W., & Bortnik, J. (2020). Global model of whistler mode chorus in the near-equatorial region ($|\lambda m| < 18°$). *Geophysical Research Letters*, *47*(11), e2020GL087311. https://doi.org/10.1029/2020GL087311

Miyoshi, Y., Sakaguchi, K., Shiokawa, K., Evans, D., Albert, J., Connors, M., & Jordanova, V. (2008). Precipitation of radiation belt electrons by EMIC waves, observed from ground and space. *Geophysical Research Letters*, *35*(23), L23101. https://doi.org/10.1029/2008GL035727

Ni, B., Cao, X., Zou, Z., Zhou, C., Gu, X., Bortnik, J., et al. (2015). Resonant scattering of outer zone relativistic electrons by multiband EMIC waves and resultant electron loss time scales. *Journal of Geophysical Research: Space Physics*, *120*(9), 7357–7373. https://doi.org/10.1002/2015JA021466

Ni, B., Thorne, R. M., Zhang, X., Bortnik, J., Pu, Z., Xie, L., et al. (2016). Origins of the Earth's diffuse auroral precipitation. *Space Science Reviews*, *200*(1–4), 205–259. https://doi.org/10.1007/s11214-016-0234-7

Onsager, T. G., Green, J. C., Reeves, G. D., & Singer, H. J. (2007). Solar wind and magnetospheric conditions leading to the abrupt loss of outer radiation belt electrons. *Journal of Geophysical Research*, *112*(A1), A01202. https://doi.org/10.1029/2006JA011708

Onsager, T. G., Rostoker, G., Kim, H.-J., Reeves, G. D., Obara, T., Singer, H. J., & Smithtro, C. (2002). Radiation belt electron flux dropouts: Local time, radial, and particle-energy dependence. *Journal of Geophysical Research*, *107*(A11), 1382. https://doi.org/10.1029/2001JA000187

Ozeke, L. G., Mann, I. R., Dufresne, S. K. Y., Olifer, L., Morley, S. K., Claudepierre, S. G., et al. (2020). Rapid outer radiation belt flux dropouts and fast acceleration during the March 2015 and 2013 storms: The role of ULF wave transport from a dynamic outer boundary. *Journal of Geophysical Research: Space Physics*, *125*(2), e2019JA027179. https://doi.org/10.1029/2019JA027179

Ozeke, L. G., Mann, I. R., Murphy, K. R., Sibeck, D. G., & Baker, D. N. (2017). Ultra-relativistic radiation belt extinction and ULF wave radial diffusion: Modeling the September 2014 extended dropout event. *Geophysical Research Letters*, *44*(6), 2624–2633. https://doi.org/10.1002/2017GL072811

Paral, J., Hudson, M. K., Kress, B. T., Wiltberger, M. J., Wygant, J. R., & Singer, H. J. (2015). Magnetohydrodynamic modeling of three Van Allen Probes storms in 2012 and 2013. *Annales Geophysicae*, *33*(8), 1037–1050. https://doi.org/10.5194/angeo-33-1037-2015

Pierrard, V., Ripoll, J.-F., Cunningham, G., Botek, E., Santolik, O., Thaller, S., et al. (2021). Observations and simulations of dropout events and flux decays in October 2013: Comparing MEO equatorial with LEO polar orbit. *Journal of Geophysical Research: Space Physics*, *126*(6), e2020JA028850. https://doi.org/10.1029/2020JA028850

Reeves, G. D., Friedel, R. H. W., Larsen, B. A., Skoug, R. M., Funsten, H. O., Claudepierre, S. G., et al. (2016). Energy-dependent dynamics of keV to MeV electrons in the inner zone, outer zone, and slot regions. *Journal of Geophysical Research: Space Physics*, *121*(1), 397–412. https://doi.org/10.1002/2015JA021569

Reeves, G. D., McAdams, K. L., Friedel, R. H. W., & O'Brien, T. P. (2003). Acceleration and loss of relativistic electrons during geomagnetic storms. *Geophysical Research Letters*, *30*(10), 1529. https://doi.org/10.1029/2002GL016513

Ripoll, J.-F., Claudepierre, S. G., Ukhorskiy, A. Y., Colpitts, C., Li, X., Fennell, J., & Crabtree, C. (2020). Particle dynamics in the Earth's radiation belts: Review of current research and open questions. *Journal of Geophysical Research: Space Physics*, *125*(5), e2019JA026735. https://doi.org/10.1029/2019JA026735

Rodger, C. J., Hendry, A. T., Clilverd, M. A., Kletzing, C. A., Brundell, J. B., & Reeves, G. D. (2015). High-resolution in situ observations of electron precipitation-causing EMIC waves. *Geophysical Research Letters*, *42*(22), 9633–9641. https://doi.org/10.1002/2015GL066581

Sergeev, V. A., & Tsyganenko, N. A. (1982). Energetic particle losses and trapping boundaries as deduced from calculations with a realistic magnetic field model. *Planetary and Space Science*, *30*(10), 999–1006. https://doi.org/10.1016/0032-0633(82)90149-0

Shprits, Y. Y., Thorne, R. M., Friedel, R., Reeves, G. D., Fennell, J., Baker, D. N., & Kanekal, S. G. (2006). Outward radial diffusion driven by losses at magnetopause. *Journal of Geophysical Research*, *111*(A11), A11214. https://doi.org/10.1029/2006JA011657

Smith, D. M., Casavant, E. P., Comess, M. D., Liang, X., Bowers, G. S., Selesnick, R. S., et al. (2016). The causes of the hardest electron precipitation events seen with SAMPEX. *Journal of Geophysical Research: Space Physics*, *121*(9), 8600–8613. https://doi.org/10.1002/2016JA022346

Spence, H. E., Reeves, G. D., Baker, D. N., Blake, J. B., Bolton, M., Bourdarie, S., et al. (2013). Science goals and overview of the energetic particle, composition, and thermal plasma (ECT) suite on NASA's radiation belt storm Probes (RBSP) mission. *Space Science Reviews*, *179*(1–4), 311–336. https://doi.org/10.1007/s11214-013-0007-5

Staples, F. A., Kellerman, A., Murphy, K. R., Rae, I. J., Sandhu, J. K., & Forsyth, C. (2022). Resolving magnetopause shadowing using multi-mission measurements of phase space density. *Journal of Geophysical Research: Space Physics*, *127*(2), e2021JA029298. https://doi.org/10.1029/2021JA029298

Su, Z., Gao, Z., Zhu, H., Li, W., Zheng, H., Wang, Y., et al. (2016). Nonstorm time dropout of radiation belt electron fluxes on 24 September 2013. *Journal of Geophysical Research: Space Physics*, *121*(7), 6400–6416. https://doi.org/10.1002/2016JA022546

Summers, D., Ma, C., Meredith, N. P., Horne, R. B., Thorne, R. M., Heynderickx, D., & Anderson, R. R. (2002). Model of the energization of outer-zone electrons by whistler-mode chorus during the October 9, 1990 geomagnetic storm. *Geophysical Research Letters*, *29*(24), 217427-4. https://doi.org/10.1029/2002GL016039

Thorne, R. M. (2010). Radiation belt dynamics: The importance of wave-particle interactions. *Geophysical Research Letters*, *37*(22), L22107. https://doi.org/10.1029/2010GL044990

Thorne, R. M., Li, W., Ni, B., Ma, Q., Bortnik, J., Chen, L., et al. (2013). Rapid local acceleration of relativistic radiation-belt electrons by magnetospheric chorus. *Nature*, *504*(7480), 411–414. https://doi.org/10.1038/nature12889

Thorne, R. M., Ni, B., Tao, X., Horne, R. B., & Meredith, N. P. (2010). Scattering by chorus waves as the dominant cause of diffuse auroral precipitation. *Nature*, *467*(7318), 943–946. https://doi.org/10.1038/nature09467

Tsurutani, B. T., Hajra, R., Tanimori, T., Takada, A., Remya, B., Mannucci, A. J., et al. (2016). Heliospheric plasma sheet (HPS) impingement onto the magnetosphere as a cause of relativistic electron dropouts (REDs) via coherent EMIC wave scattering with possible consequences for climate change mechanisms. *Journal of Geophysical Research: Space Physics*, *121*, 10130–10156. https://doi.org/10.1002/2016JA022499

Tsyganenko, N. A., & Sitnov, M. I. (2005). Modeling the dynamics of the inner magnetosphere during strong geomagnetic storms. *Journal of Geophysical Research*, *110*(A3), A03208. https://doi.org/10.1029/2004JA010798

Tu, W., Cunningham, G. S., Chen, Y., Morley, S. K., Reeves, G. D., Blake, J. B., et al. (2014). Event-specific chorus wave and electron seed population models in DREAM3D using the Van Allen Probes. *Geophysical Research Letters*, *41*(5), 1359–1366. https://doi.org/10.1002/2013GL058819

Tu, W., Xiang, Z., & Morley, S. K. (2019). Modeling the magnetopause shadowing loss during the June 2015 dropout event. *Geophysical Research Letters*, *46*(16), 9388–9396. https://doi.org/10.1029/2019GL084419

Turner, D. L., Angelopoulos, V., Morley, S. K., Henderson, M. G., Reeves, G. D., Li, W., et al. (2014). On the cause and extent of outer radiation belt losses during the 30 September 2012 dropout event. *Journal of Geophysical Research: Space Physics*, *119*(3), 1530–1540. https://doi.org/10.1002/2013JA019446

Turner, D. L., Kilpua, E. K. J., Hietala, H., Claudepierre, S. G., O'Brien, T. P., Fennell, J. F., et al. (2019). The response of Earth's electron radiation belts to geomagnetic storms: Statistics from the Van Allen Probes era including effects from different storm drivers. *Journal of Geophysical Research: Space Physics*, *124*(2), 1013–1034. https://doi.org/10.1029/2018JA026066

Turner, D. L., Morley, S. K., Miyoshi, Y., Ni, B., & Huang, C.-L. (2012). Outer radiation belt flux dropouts: Current understanding and unresolved questions. In D. Summers, I. R. Mann, D. N. Baker, & M. Schulz (Eds.), *Dynamics of the Earth's radiation belts and inner magnetosphere*. https://doi.org/10.1029/2012GM001310

Turner, D. L., O'Brien, T. P., Fennell, J. F., Claudepierre, S. G., Blake, J. B., Kilpua, E. K. J., & Hietala, H. (2015). The effects of geomagnetic storms on electrons in Earth's radiation belts. *Geophysical Research Letters*, *42*(21), 9176–9184. https://doi.org/10.1002/2015gl064747

Turner, D. L., Shprits, Y., Hartinger, M., & Angelopoulos, V. (2012). Explaining sudden losses of outer radiation belt electrons during geomagnetic storms. *Nature Physics*, *8*(3), 208–212. https://doi.org/10.1038/nphys2185

Ukhorskiy, A. Y., Anderson, B. J., Brandt, P. C., & Tsyganenko, N. A. (2006). Storm time evolution of the outer radiation belt: Transport and losses. *Journal of Geophysical Research*, *111*(A11), A11S03. https://doi.org/10.1029/2006JA011690

Usanova, M. E., Drozdov, A., Orlova, K., Mann, I. R., Shprits, Y., Robertson, M. T., et al. (2014). Effect of EMIC waves on relativistic and ultrarelativistic electron populations: Ground-based and Van Allen Probes observations. *Geophysical Research Letters*, *41*(5), 1375–1381. https://doi.org/10.1002/2013GL059024

Xiang, Z., Tu, W., Li, X., Ni, B., Morley, S. K., & Baker, D. N. (2017). Understanding the mechanisms of radiation belt dropouts observed by Van Allen Probes. *Journal of Geophysical Research: Space Physics*, *122*(10), 9858–9879. https://doi.org/10.1002/2017JA024487

Xiang, Z., Tu, W., Ni, B., Henderson, M. G., & Cao, X. (2018). A statistical survey of radiation belt dropouts observed by Van Allen Probes. *Geophysical Research Letters*, *45*(16), 8035–8043. https://doi.org/10.1029/2018GL078907

Yahnin, A. G., Yahnina, T. A., Raita, T., & Manninen, J. (2017). Ground pulsation magnetometer observations conjugated with relativistic electron precipitation. *Journal of Geophysics Research: Space Physics*, *122*(9), 9169–9182. https://doi.org/10.1002/2017JA024249

Yahnin, A. G., Yahnina, T. A., Semenova, N. V., Gvozdevsky, B. B., & Pashin, A. B. (2016). Relativistic electron precipitation as seen by NOAA POES. *Journal of Geophysical Research: Space Physics*, *121*(9), 8286–8299. https://doi.org/10.1002/2016JA022765

Yuan, C., & Zong, Q. (2013). Relativistic electron fluxes dropout in the outer radiation belt under different solar wind conditions. *Journal of Geophysical Research: Space Physics*, *118*(12), 7545–7556. https://doi.org/10.1002/2013JA019066

Zhang, X.-J., Li, W., Ma, Q., Thorne, R. M., Angelopoulos, V., Bortnik, J., et al. (2016). Direct evidence for EMIC wave scattering of relativistic electrons in space. *Journal of Geophysical Research: Space Physics*, *121*(7), 6620–6631. https://doi.org/10.1002/2016JA022521

Zhang, X.-J., Li, W., Thorne, R. M., Angelopoulos, V., Ma, Q., Li, J., et al. (2016). Physical mechanism causing rapid changes in ultrarelativistic electron pitch angle distributions right after a shock arrival: Evaluation of an electron dropout event. *Journal of Geophysical Research: Space Physics*, *121*(9), 8300–8316. https://doi.org/10.1002/2016JA022517

Zhang, X.-J., Mourenas, D., Artemyev, A. V., Angelopoulos, V., & Thorne, R. M. (2017). Contemporaneous EMIC and whistler mode waves: Observations and consequences for MeV electron loss. *Geophysical Research Letters*, *44*(16), 8113–8121. https://doi.org/10.1002/2017GL073886